Applied Catalysis B: Environmental 305 (2022) 121043

Contents lists available at ScienceDirect

Applied Catalysis B: Environmental

journal homepage: www.elsevier.com/locate/apcatb

# Metal-organic frameworks derived $RuP_2$ with yolk-shell structure and efficient performance for hydrogen evolution reaction in both acidic and alkaline media

Jiahuan Luo [a,b], Jing Wang [b,*], Yao Guo [b], Jiawei Zhu [a], Huihui Jin [a], Zhiwei Zhang [a], Daojun Zhang [c], Yongsheng Niu [b], Shaogang Hou [b], Jimin Du [c], Daping He [a], Yuli Xiong [d], Lei Chen [a], Shichun Mu [a,e,**], Yunhui Huang [f]

[a] State Key Laboratory of Advanced Technology for Materials Synthesis and Processing, Wuhan University of Technology, Wuhan 430070, PR China
[b] School of Chemical and Environmental Engineering, Anyang Institute of Technology, Anyang 455000, PR China
[c] College of Chemistry and Chemical Engineering, Anyang Normal University, Anyang 455000, PR China
[d] School of Materials Science and Engineering, Wuhan University of Technology, Wuhan 430070, PR China
[e] Foshan Xianhu Laboratory of the Advanced Energy Science and Technology Guangdong Laboratory, Xianhu Hydrogen Valley, Foshan 528200, PR China
[f] State Key Laboratory of Material Processing and Die & Mould Technology, School of Materials Science and Engineering, Huazhong University of Science and Technology, Wuhan 430074, PR China

ARTICLE INFO

*Keywords:*
Metal-organic frameworks
Ruthenium di-phosphide
DFT calculation
Hydrogen evolution reaction
Yolk-shell structure

ABSTRACT

Hydrogen generation from electrical water splitting has become a greatly increasing requirement for energy systems, however, highly effective and durable electrocatalysts towards universal-pH hydrogen evolution reaction (HER) remain a big challenge. Herein, we design and synthesize ruthenium di-phosphide ($RuP_2$) confined in carbon layers ($RuP_2$-C) with a unique yolk-shell structure ($RuP_2$-C@$RuP_2$-C) from MOF. As expected, it not only exceeds the HER activity of Pt catalysts, with very tiny overpotentials at 10 mA $cm^{-2}$ (9 and 17 mV in 1.0 M KOH and 0.5 M $H_2SO_4$, individually), but also has high stability. Besides, it also exhibits a low overpotential (40 mV) close to Pt catalysts and high stability in 1.0 M PBS, indicating that $RuP_2$-C@$RuP_2$-C (RPC@RPC) owns outstanding HER performance at all pH values. Density functional theory (DFT) calculation results further unravel that the P-site on the surface of RPC@RPC possesses low hydrogen adsorption energy, beneficial for boosting the HER activity.

## 1. Introduction

Hydrogen energy is considered as one of most influential energy candidates for traditional fossil fuels, which will become the predominant clean renewable energy source because of its sustainability and environmentally friendly properties [1–5]. Electrical driven water electrolysis is an environmentally friendly and continuable method for hydrogen generation [6–8], however, it requires the high overpotential for water-splitting reactions, which increases the energy consumption. Thus, it is very demanded to seek for an expeditious electrocatalyst towards hydrogen evolution reaction (HER). As an energy-efficient electrocatalyst for HER, it should activate the proton reduction with minimum overpotentials and enhanced kinetics. Hitherto, the platinum (Pt)-based material is still the best electrocatalysts for HER because of low HER overpotentials, high exchange current densities and small Tafel slopes. Unfortunately, suffering from the scarcity, costly expenses and poor electro-chemical stability, the extensive application of Pt-based electrocatalysts is limited seriously [9–14]. As a result, a lot of non-noble metal materials have been researched as promising candidates [15–22], however, their activity towards HER is still far from satisfaction compared to Pt in wide pH ranges. Therefore, it is still an ongoing urgent task to explore novel cost-effectively electrocatalysts with catalysis liveness as same as Pt for HER in overall pH ranges.

Ru-based electrocatalysts have attracted great attentions recently not

* Corresponding author.
** Corresponding author at: State Key Laboratory of Advanced Technology for Materials Synthesis and Processing, Wuhan University of Technology, Wuhan 430070, PR China.
*E-mail addresses:* wangjing2017@ayit.edu.cn (J. Wang), msc@whut.edu.cn (S. Mu).

https://doi.org/10.1016/j.apcatb.2021.121043
Received 29 October 2021; Received in revised form 15 December 2021; Accepted 22 December 2021
Available online 24 December 2021

only because of lower price of Ru over other Pt-group metals, but also due to their Pt-like electrocatalysis performance [23–41]. What's more, based on the fact that Ru can easily coordinate to oxygen, accordingly, the introduction of Ru could enhance the alkaline HER catalytic activity of Pt-series materials based on the 'Water dissociation theory' [6,7]. Besides that the metallic Ru or Ru-doped alloy shows a fundamentally modest HER activity, other Ru-based materials, especially those coordinated with nanocarbons, nitrogen, boron and phosphorus can also display excellent HER capability similar to or even better than Pt catalysts. Recently, Ruthenium phosphide compounds have been investigated a lot. Cai's group [39] reported a Ru-$Ru_2P$/PC catalyst which showed high HER activity in alkaline condition. Our group synthesized $RuP_2$ @NPC catalysts using the coordination of phytic acid and Ru, indicating that the P-rich $RuP_2$ @NPC can efficiently increase the adsorption capacity of hydrogen and improve the HER activity. However, in the existing synthetic strategy, the active sites of the catalyst are always wrapped in depth of the surface, resulting in less exposed catalytic active sites and lower mass activity of $RuP_2$. Therefore, the controllable design of low level $RuP_2$ dispersed on porous carbon with extensive exposed active sites is significant and urgent.

Metal-organic frameworks (MOFs), with fascinating structural diversity, tailor-ability and chemical multiformity, have been used to construct MOFs derivatives with rich pores, high definite surface area, order pore canals and regular shape, exhibiting high electrocatalysis activity [42–47]. So far as we know, only few Ru-MOFs are used to synthesize the ruthenium phosphide [41], thus, in this work, by combining the advantage of $RuP_2$ and MOFs, we take Ru-MOFs (Ru-H-KUST-1) [48] as template to design and construct P-doped carbon encapsulated $RuP_2$ with unique yolk-shell structure ($RuP_2$-C@$RuP_2$-C). This allows $RuP_2$-C@$RuP_2$-C (defined as RPC@RPC) with high surface area and rich active sites in comparison with pure $RuP_2$ by taking advantage of the space of hollow $RuP_2$-C spheres, beneficial for improvement of electrocatalysis. Expectably, as HER electrocatalyst, it displays fantastic electrocatalytic performance at all pH values. The DFT calculation results further demonstrate that the P site of carbon surface in RPC@RPC has an optimal hydrogen adsorption Gibbs free energy ($\Delta G_{H^*}$) value, in favor of enhancing HER activity.

## 2. Experimental section

### 2.1. Materials

$RuCl_3{\cdot}xH_2O$, $RuO_2$, 1,3,5-benzenetricarboxylic acid ($H_3BTC$), KOH, $H_2SO_4$, $Na_2HPO_4{\cdot}12H_2O$ $NaH_2PO_4{\cdot}2H_2O$, $NaH_2PO_2{\cdot}H_2O$, isopropyl alcohol, alcohol, and glacial acetic acid ($HA_c$) were purchased from Aladdin Reagents Ltd. Pt/C (20 wt%), F-127 and Nafion (5 wt%) were purchased from Sigma-Aldrich. All of the reagents are analytical grade and used without further purification. De-ionized water was obtained from an ultra-pure purifier (Ulupure, China, resistivity $\geq$ 18.2 MΩ).

### 2.2. Synthesis of Ru-MOF

Ru-MOF were synthesized by an ordinary hydrothermal method. $RuCl_3.3\,H_2O$ (300 mg), $H_3BTC$ (200 mg), F-127 (200 mg) and Acetic acid (1.2 mL) were added into 40 mL ultrapure water in an 100 mL Teflon-lined autoclave and stirred for half hour, then heated at 160 °C for 72 h. After natural cooling, centrifuging and filtering, washing with De-ionized water and alcohol separately for three times to get a light-green powder, and the yield Ru-MOF is pretty high.

### 2.3. Synthesis of RPC@RPC

The ceramic boat with as-prepared Ru-MOF (20 mg) was put to the middle of the tube furnace, with $NaH_2PO_2$ (200 mg) at the upstream side of the furnace. Then, they were pyrolyzed at 700 °C for 2 h with a heating rate of 5 °C $min^{-1}$ under a 5% hydrogen-argon gas mixture. After being cooling to room temperature, the product was collected and washed by centrifugation with alcohol and water three times to remove the residue of reactants, and finally dried in vacuum at 80 °C overnight. Finally, the black powder of RPC@RPC was obtained. **Caution:** To eliminate the toxic $PH_3$ gas, the tail gas produced in the phosphatizing process was firstly dealt with the saturated $CuSO_4$ solution and then the saturated $Fe(NH_3)_2(SO_4)_2$ solution. The synthesis of $RuP_2$ was similar to RPC@RPC but use commercial $RuCl_3$ as Ru resource.

### 2.4. Preparation the working electrode

5.0 mg of the catalyst powder was dispersed in 490 μL isopropanol/water (v/v=10:1) mixed solvents along with 10 μL 5 wt% of Nafion solution, and the mixed solution was sonicated for 30 min. Then 6 μL of the catalyst ink was loaded on a glassy carbon electrode (GCE: diameter = 3 mm) at a catalyst loading of 0.85 mg $cm^{-2}$.

### 2.5. Material characterization

Transmission electron microscopy (TEM), high-angle annular dark-field scanning TEM (HAADF-STEM), high-resolution transmission electron microscopy (HRTEM), and energy dispersive X-Ray spectroscopy (EDX) were carried out on a FEI Talos F200s TEM (200 kV). Power X-ray diffraction (PXRD) patterns were collected from a Bruker powder diffractometer with Cu radiation (λ = 0.15406 nm). X-ray photoelectron spectroscopy (XPS) tests were carried out with Thermo Scientifc Escalab 250Xi using a monochromated Al-Kα (1486.5 eV) X-ray radiation. All the binding energies were calibrated to C 1 s adventitious carbon at 284.8 eV to eliminate differences in sample charging. The CP-OES was carried out on Agilent 5100 ICP-OES.

### 2.6. Electrocatalytic HER tests

All electrochemical measurements were performed on a CHI-760E electrochemical analyzer (CH Instruments, Inc., Shanghai) in a standard 3-electrode cell. The acidic (0.5 M $H_2SO_4$) and neutral (1.0 M PBS) electrochemical measurements were performed using a saturated calomel electrode (SCE) as the reference electrode. The alkaline (1.0 M KOH) electrochemical measurements were carried out using a Hg/HgO as the reference electrode. A graphite rod was used as the counter electrode in all measurements. Polarization data were obtained at a scan rate of 2 mV $s^{-1}$. In all measurements, the reference electrode was calibrated with respect to reversible hydrogen electrode (RHE). The current-voltage was run at a scan rate of 2 mV $s^{-1}$, and the average of the two potentials at which the current crossed zero was taken to be the thermo-dynamic potential for the H-electrode reactions. All polarization curves were iR-corrected. Electrochemical impedance spectroscopy (EIS) measurements were carried out in the frequency range of 100 kHz–0.01 Hz with AC amplitude of 10 mV.

## 3. Results and discussion

### 3.1. Synthesis and structural characterization

As illustrated in Fig. 1a, $RuP_2$ was synthesized via a two-step chemical procedure. Firstly, Ru-MOF was prepared by an ordinary hydrothermal reaction with $RuCl_3$, 1, 3, 5-benzenetricarboxylic acid ($H_3BTC$), F-127 and glacial acetic acid as raw materials. Then, the prepared Ru-MOF was converted to a yolk-shell structure with $RuP_2$ and carbon coatings by using $NaH_2PO_2$ as the phosphating agent in tubular furnace under $H_2$/Ar atmosphere at target temperatures (700 °C), the obtained sample was marked as $RuP_2$-C@$RuP_2$-C (RPC@RPC). As a contrast, the pure $RuP_2$ was synthesized in the same condition as RPC@RPC by phosphating $RuCl_3$. The high phase purity of the Ru-MOF was confirmed by the X-ray powder diffraction (XRD), all the diffraction peaks are consistent with that of the simulated HKUST-1 patterns

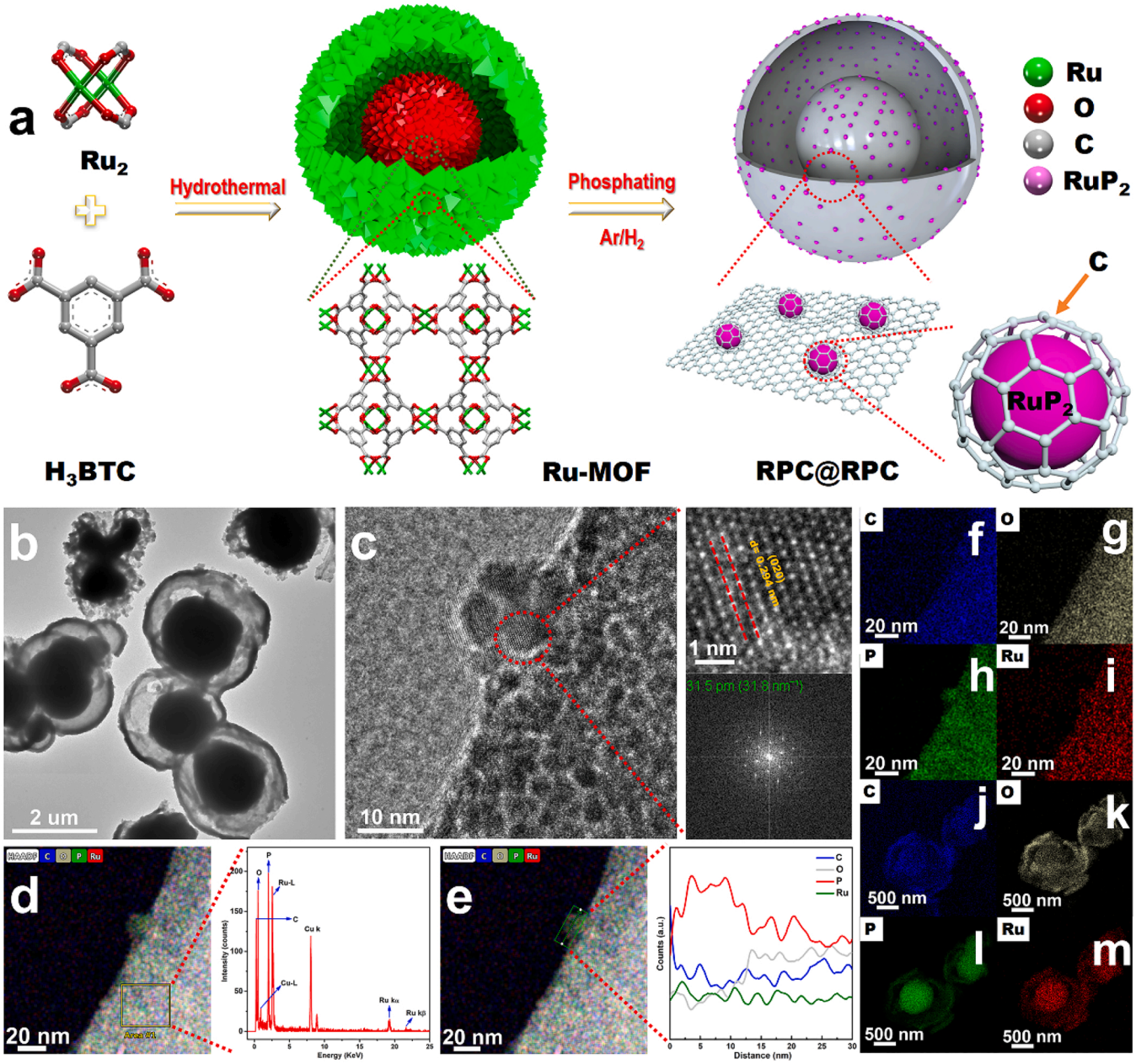


**Fig. 1.** (a) Scheme of the synthetic route for preparation of RPC@RPC. (b) TEM images, (c) HRTEM images, (d) HAADF-STEM EDX, (e) HAADF-STEM-EDX line scans, HAADF-STEM image and elemental mapping for RPC@RPC (C, O, P, and Ru) in small size (f–i) and large size (j-m).

(Fig. S1).

As demonstrated in Figs. S2, S3, the morphology of Ru-MOF, $RuP_2$ and RPC@RPC was examined by scanning electron microscopy (SEM). SEM images display that Ru-MOF are present in sphere-like particles with diameter of 3–4 μm, which are assembled by smaller crystals with size of 100 nm. After pyrolysis, the shape of etched spheres in the surface and egg-shells occur for RPC@RPC. Furthermore, TEM, HAADF-STEM, and HRTEM were executed to identify the structure of Ru-MOFs and RPC@RPC materials. Fig. S4 shows that the as-synthesized Ru-MOF particles have an average diameter of 3–4 μm, and consist of Ru-MOF single-crystals with diameter of 100 nm. Furthermore, it can be observed that Ru-MOF particles have a yolk-shell structure. The HAADF-STEM image and the corresponding EDS elemental mapping show the homogeneous dispersion of the C, O and Ru elements throughout the whole structure (Figs. S4d-4f). Fig. 1b and S5 demonstrate that RPC@RPC also possesses a typical yolk-shell structure like Ru-MOFs with 1.5–2 μm solid core and 3–4 μm etched shell. Fig. 1c further exhibits the homogeneous distribution of $RuP_2$ @C with a mean size of ≈ 7 nm, with the distinct lattice spacing of d = 2.93 Å which corresponds to the $RuP_2$ (020) facet, and Fig. S6 show that $RuP_2$@C has distinct lattice spacing of d = 3.85 Å which corresponds to the $RuP_2$ (110) facet. HAADF-STEM-EDX line scans ulterior substantiate that $RuP_2$ is well wrapped with carbon layers (Fig. 1d, e). In addition, from HAADF-STEM EDX elemental mapping (Fig. 1f-m, S5), it shows the well-proportioned distribution of C, P, O and Ru in RPC@RPC. More importantly, from Fig. 1j–m and S5c, it is further intuitively confirmed that RPC@RPC owns a typical yolk-shell structure, in which both of the solid core and etched shell are composed of RPC, namely the P-doped carbon encapsulated $RuP_2$. The inductively coupled plasma optical emission spectrometer (ICP-OES) test presents the Ru content of 20.2 wt % in RPC@RPC.

All the XRD peaks of $RuP_2$ and RPC@RPC in Fig. 2a are indexed to

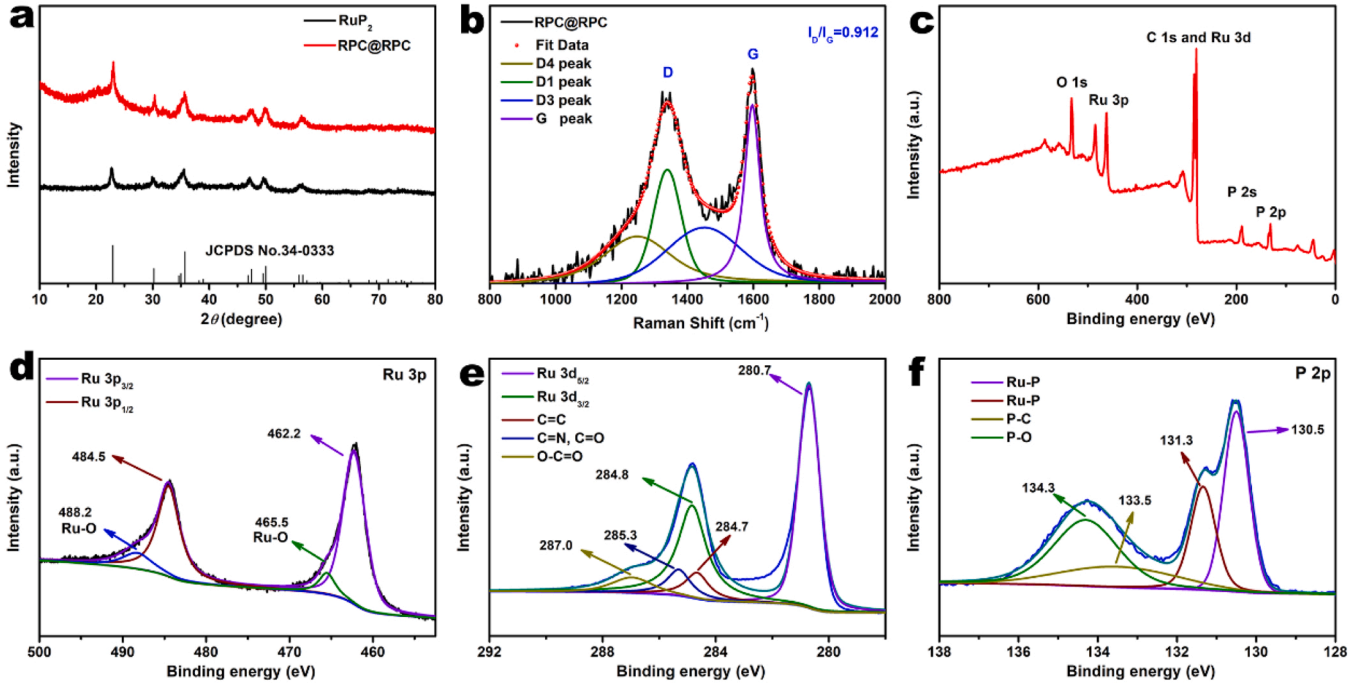


**Fig. 2.** (a) XRD pattern, (b) Raman spectrum and (c-f) XPS survey pattern of RPC@RPC.

the phase-pure $RuP_2$ (JCPDS No. 34-0333). In the Raman spectrum (Fig. 2b), for RPC@RPC the peaks at ~ 1338 and ~ 1596 $cm^{-1}$ ascribed to D and G bands of carbon component separately deliver a low peak intensity ratio ($I_D/I_G$ = 0.91), indicating the high graphitization of carbon in RPC@RPC. In addition, XPS was performed to study the specific elementary constituent and surface compound state of RPC@RPC. It shows that the surface elemental composition of RPC@RPC is C, P, O and Ru (Fig. 2c–f). The peaks at 462.2 eV, 484.5 eV correspond to the binding energy (BE) of Ru $3p_{3/2}$ and Ru $3p_{1/2}$ of RPC@RPC, while the other two peaks at 465.5 and 488.2 eV correspond to the Ru oxide species [41]. The peaks of 280.7 eV, 284.8 eV belong to Ru $3d_{5/2}$, Ru $3d_{3/2}$ of RPC@RPC, individually, while they are assigned to C═C, C═N/C═O and C-C═O at 284.7, 285.3 and 287.0 eV [24], respectively (Fig. 2e). What's more, Fig. 2f displays the P 2p spectrum, in which the peaks at 133.5 eV, 134.3 eV are assigned to P-O and P-C, respectively, and the peaks at 131.3 eV and 130.5 eV are ascribed to Ru-P [39]. All the essential characterizations above containing TEM, HRTEM, SEM, XRD, Raman and XPS reveal the successful synthesis of RPC@RPC.

$N_2$ adsorption isotherms for samples are shown in Fig. S7 the Brunauer-Emmett-Teller (BET) for RPC@RPC has a typical type-IV curve and $H_{III}$-type hysteresis loop, suggesting the occurrence of micropores and mesopores in RPC@RPC. Its specific surface area and pore volume are 45.5 $m^2$ $g^{-1}$ and 0.0934 $cm^3$ $g^{-1}$ $nm^{-1}$, respectively. This porous structure greatly increases the surface area and mass transfer capability of catalysts, beneficial for HER.

### 3.2. Hydrogen evolution catalysis

The electrocatalytic HER performance for RPC@RPC and benchmarks was investigated, with a scan rate of 2 mV $s^{-1}$ in a 1 M KOH three-electrode electrochemical system at 25 °C. The HER activity in sequence is RPC@RPC > Pt/C > $RuP_2$ (Fig. 3a). Amazingly, the overpotential of RPC@RPC was calculated to be only 9 mV (10 mA $cm^{-2}$, $j_{10}$) lower than Pt/C ($j_{10}$ = 27 mV) and $RuP_2$ ($j_{10}$ = 102 mV), even much lower than $RuP_2$ @NPC ($j_{10}$ = 52 mV) we reported previously [24]. Moreover, the pristine polarization curves without iR-correction are shown in Fig. S8a. What's more, it is extremely valuable referring that RPC@RPC exhibits the overpotential of 23 mV at $j_{50}$ and 35 mV at $j_{100}$, much lower than most catalytic materials (Fig. 3b, Table S1). As indicated in Fig. 3c, the Tafel slopes of RPC@RPC, $RuP_2$ and Pt/C are 15, 30 and 52 mV $dec^{-1}$, respectively, implying that RPC@RPC owns more desirable kinetics than Pt/C and $RuP_2$. Such small overpotentials and Tafel slopes of RPC@RPC in alkaline media conditions indicate it possesses HER activity outperforming Pt catalysts and most of HER catalysts have been reported up to now (Table S1).

Besides the catalytic activity, the electrochemical stability is an imperative parameter for the industrial application of catalysts. Afterwards 10,000 cyclic voltammetric (CV) cycles in alkaline condition, as displayed in Fig. 3d, the increased overpotentials are 4 mV at $j_{10}$ and 19 mV at $j_{100}$. At the same time, it displays an excellent durability with hardly any current density attenuation over 20 h (inset of Fig. 3d). After the durability test, the catalyst was collected to characterize. Its XRD pattern indicates RPC@RPC still maintains an initial crystalline structure. The comparability of Ru 3d and P 2p from XPS spectra (Fig. S9) of after HER RPC@RPC confirms the retentivity of the catalyst conformation, substantiating the splendid stableness. In addition, the TEM observation demonstrates that $RuP_2$ still keeps good dispersion in catalysts, without any obvious accumulation and movement (Fig. S10), proving the high stability of RPC@RPC catalysts. All of these above results reveal that RPC@RPC with a yolk-shell structure is indeed a highly effective and enduring catalyst for HER in 1 M KOH solutions.

Besides the base condition, the HER performance of RPC@RPC was then examined in 0.5 M $H_2SO_4$ and 1.0 M PBS at 25 °C with same scan rate in alkaline solutions. The catalytic activity under acid media in sequence is RPC@RPC > Pt/C > $RuP_2$, similar to that in alkaline solutions (Fig. 4a–c). The overpotential of RPC@RPC was discovered to be 17 mV at $j_{10}$, even lower than Pt/C ($j_{10}$ = 47 mV) and $RuP_2$ ($j_{10}$ = 90 mV). And the origin polarization curves without iR-correction were displayed in Fig. S8b. This overpotential value is lower than that of $RuP_2$ @NPC ($j_{10}$ = 38 mV) we reported previously [24] and other catalysts (Fig. 4a, Table S1). As displayed in Fig. 4b, the Tafel slopes of RPC@RPC, $RuP_2$ and Pt/C are 19, 100, and 27 mV $dec^{-1}$, respectively, implying that RPC@RPC possesses the fastest kinetics among HER catalysts in acid media. (Table S1) It is noteworthy that the HER performance of RPC@RPC is even lower than that in basic condition, meaning that RPC@RPC can surpassingly decompose water to boost succeeding

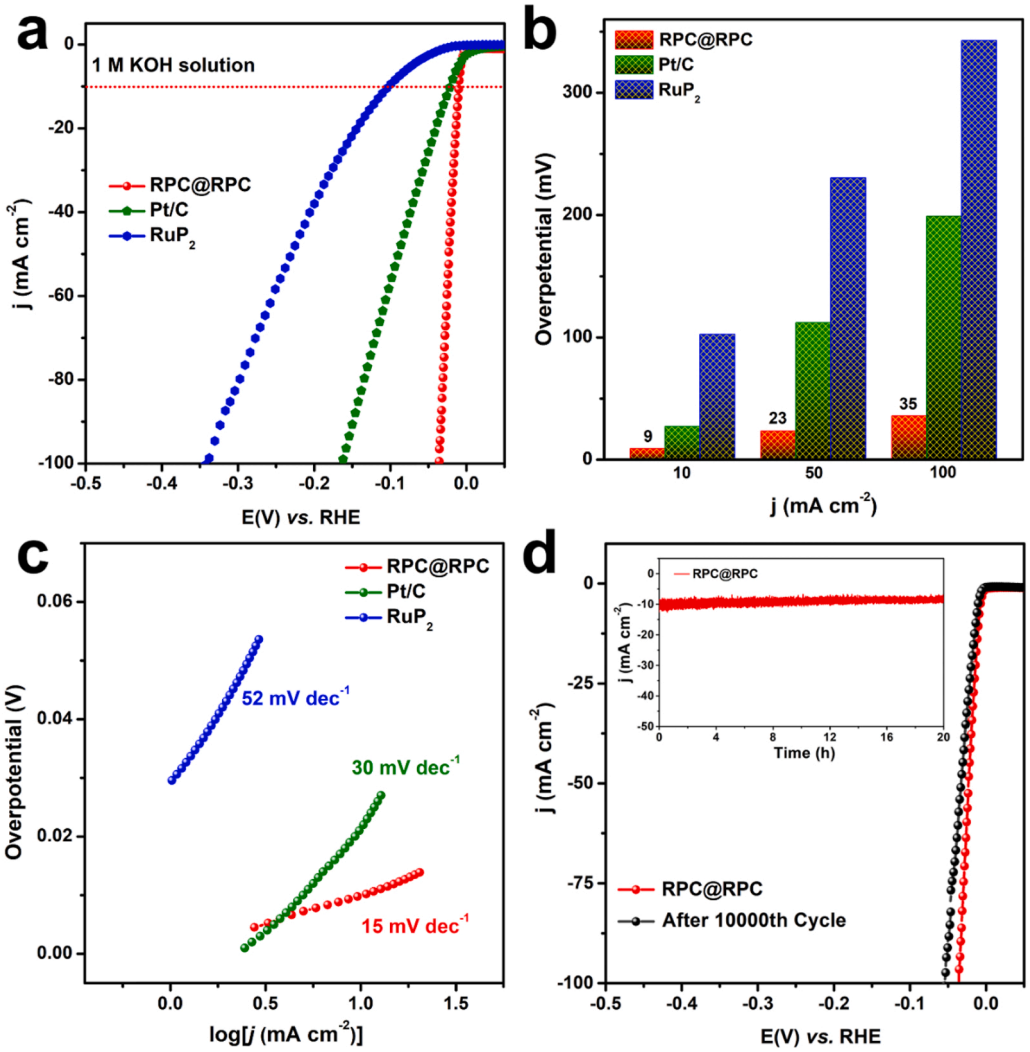


**Fig. 3.** (a) HER polarization curves, (b) Overpotentials at corresponding j (10/25/100 mA $cm^{-2}$), (c) corresponding Tafel plots for RPC@RPC, commercial Pt/C and pure $RuP_2$ in 1 M KOH, (d) Polarization curves recorded for RPC@RPC before and after 10,000 CV cycles (inset: Time-dependent current density curve of RPC@RPC).

hydrogen adsorption. This result is also consistent with recent reported work [13,34]. After 10,000 CV cycles, the increased overpotentials are only 3 mV at $j_{10}$ and 19 mV at $j_{100}$, as shown in Fig. 4c. The durability of RPC@RPC also can be confirmed by almost no current density attenuation after 20 h (Fig. 4c inset).

Furthermore, in 1 M PBS electrolytes and at $j_{10}$, RPC@RPC, Pt/C and $RuP_2$ require overpotentials of 40, 23, and 105 mV, respectively, (Fig. 4d), with the Tafel slope of 41 mV $dec^{-1}$ for RPC@RPC (Fig. 4e), indicating that RPC@RPC coincides Volmer–Heyrovsky HER mechanism [13]. Furthermore, the pristine polarization curves without iR-correction was exhibited in Fig. S8c. In addition, RPC@RPC also owns the highest TOF value (1.1 $s^{-1}$ at an HER overpotential of 100 mV) (Fig. S13). Finally, RPC@RPC also behaves high stability in neutral electrolytes, after 10,000 CV cycle and i-*t*-test for 20 h (Fig. 4f and inset).

To probe the factors which responsible for the outstanding electrocatalysis of RPC@RPC, the Nyquist plots and the electrochemical surface area (ECSA) were executed. As shown in Figs. S11 and S12, the ECSA was investigated by the double-layer capacitance ($C_{dl}$). RPC@RPC displays the larger $C_{dl}$ value of 39.69 mF $cm^{-2}$ than $RuP_2$ (2.68 mF $cm^{-2}$) (Fig. S12), corresponding a comparative ECSA (≈ 992 $cm^2$). Such high ECSA can be attributed to its porous yolk-shell structure, favoring efficient availableness of the essential active sites for HER [49]. From Nyquist plots, it reveals that the charge transfer resistance ($R_{ct}$) of RPC@RPC in alkaline, acid and neutral conditions is 7.17, 9.10 and 16.77 Ω, respectively (Fig. S11). Overall these results above, it can be determined that RPC@RPC is a highly excellent and dependable electrocatalyst for HER over a wide pH range.

### 3.3. Theoretical calculation

DFT calculations were further performed to develop comprehension of the derivation for the splendid HER performance of RPC@RPC (the computation details are shown in ESI). As we all know, the ideal catalytic site should not only have moderate adsorption energy of key intermediates, but also be dominant compared with other adjacent adsorption sites [32]. In previous work, the (110) facet was adopted to play the role of active surface for $RuP_2$ [24]. As shown in Fig. 5a, b and S14, there are at least six different sites for $H^+$ formation and adsorption, named as the Carbon-C, Carbon-P, $RuP_2$-Ru, $RuP_2$-P, RPC@RPC-C and RPC@RPC-P. As presented in Fig. 5c, the RPC@RPC-P site displays the lowest hydrogen adsorption Gibbs free energy ($\Delta G_{H^*}$) value (0.337 eV), similar to previous reports and much lower than that of the other five sites. In addition, Fig. 5d further exhibits the projected density of states (pDOS) of carbon, $RuP_2$ and RPC@RPC, demonstrating that there are DOS bonding and overlapping between the $RuP_2$ and carbon layer in RPC@RPC, promoting the electronic transfer in the HER process. Overall, the results above indicate that the excellent balance between the ligand effect and stretch in RPC@RPC affords it an appropriate

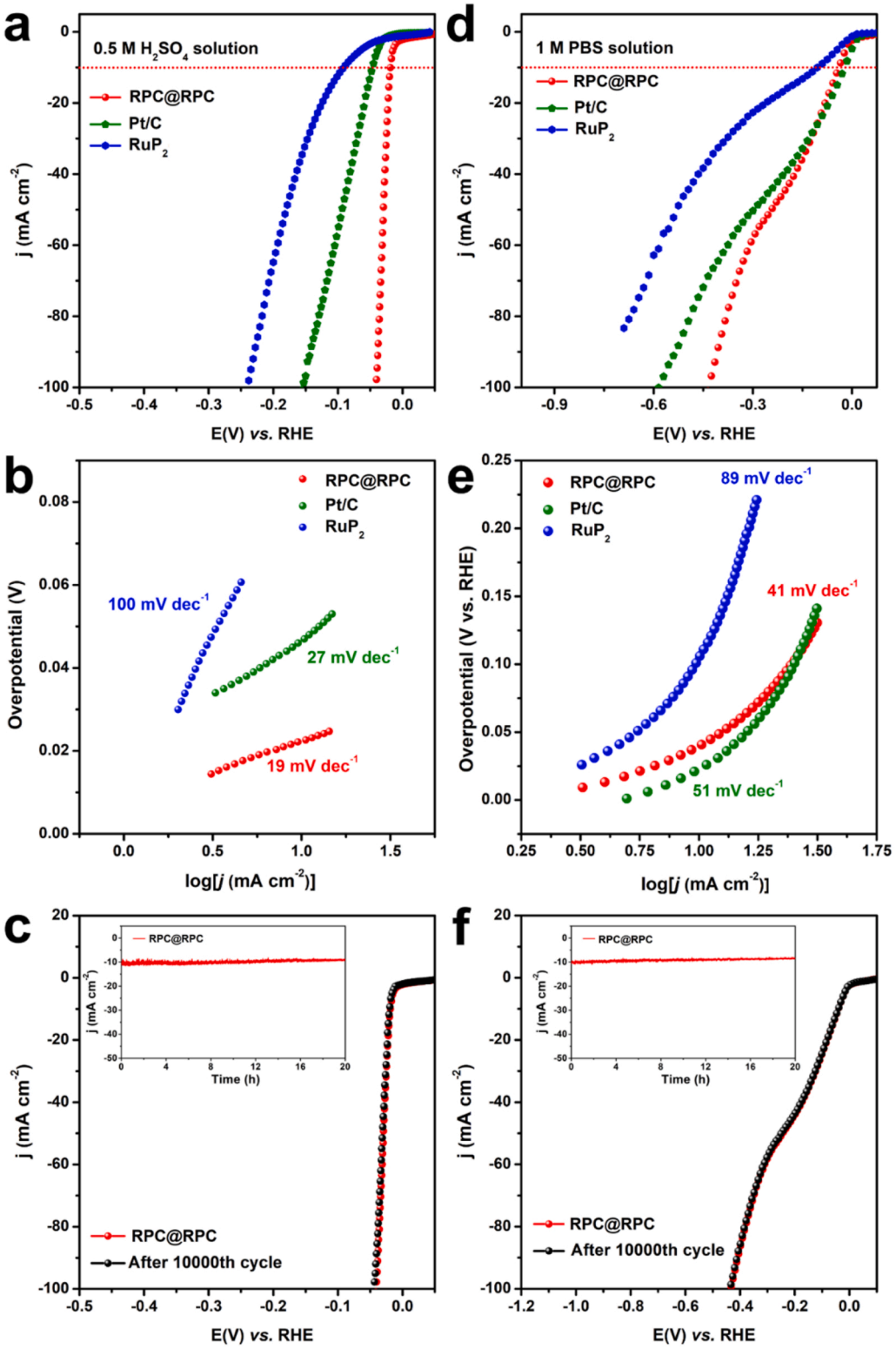


**Fig. 4.** HER polarization curves in (a) 0.5 M $H_2SO_4$, (d)1.0 M PBS, Tafel plots for RPC@RPC, commercial Pt/C and pure $RuP_2$ (b) 0.5 M $H_2SO_4$ and (e) 1.0 M PBS, Polarization curves recorded for RPC@RPC before and after 10,000 CV cycles (inset: Time-dependent current density curve of RPC@RPC) (c) 0.5 M $H_2SO_4$ and (f) 1.0 M PBS.

electronic structure and a rather low $\Delta G_H^*$ value.

By comprehensive consideration of the DFT calculation, representative constituent and unique structure of RPC@RPC, the highly efficient HER property for RPC@RPC can be attributed to the origins below: 1) the P-doped carbon in RPC@RPC modulates the electron density and modifies the electronic structure of the neighboring carbon through electronic effect, providing more active sites. 2) The synergistic reaction between $RuP_2$ NPs and wrapped carbon not only reduces the $\Delta G_{H^*}$ but also increases more catalytic sites. 3) The yolk-shell structure of RPC@RPC catalyst supplies high surface area and direct contact for

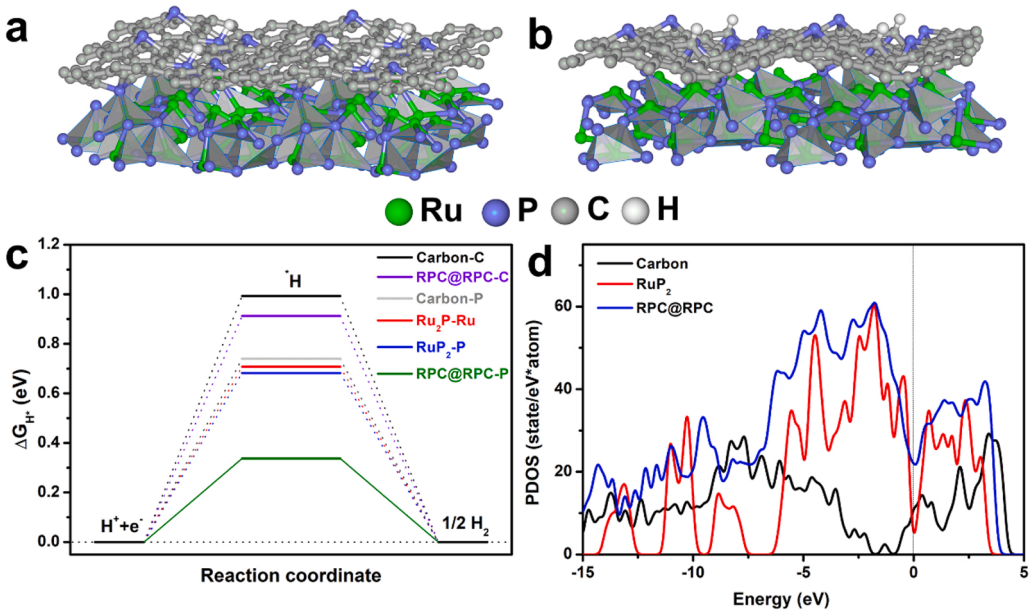


**Fig. 5.** Theoretical model of the adsorption for the H* on P sites (a) and C (b) site in carbon surface of RPC@RPC, (c) Calculated free-energy value at equilibrium potential, (d) DOS overlap and bonding for Carbon, $RuP_2$ and RPC@RPC.

yolk-shell layers, propitious for charge transfer and mass transport, further accelerating the reaction kinetics. 4) The carbon layer derived from Ru-MOF can protect catalysts from the structure collapse and prevents the $RuP_2$ from agglomerate, favorable for the long-term stability. In brief, these advantages bring the RPC@RPC with remarkable HER performance over the full pH range.

## 4. Conclusion

In summary, an effective and propagable synthesis strategy has been developed for the direct preparation of a Ru-MOF derived P-rich $RuP_2$-C@$RuP_2$-C (RPC@RPC) yolk-shell catalyst under ambient atmosphere (Ar-$H_2$) and modest processing temperatures. The as prepared catalyst, with P-doping, drastically improved pH-universal HER activity, and only required ultrasmall overpotentials of 9, 17, and 40 mV to reach a current density of 10 mA $cm^{-2}$ in 1.0 M KOH, 0.5 M $H_2SO_4$ and 1.0 M PBS electrolytes individually, exceeding most catalysts containing noble-metal, non-noble metal and nonmetal catalysts. DFT calculation results further disclosed that the improved HER capability was intensely correlated with the exposed P-site on the surface of RPC@RPC which showed a moderate hydrogen adsorption energy. Our findings supply an important route for the design and construction of high-performance pH-universal HER Ru-based and other catalysts with unique architectures by means of metal-organic frameworks.

## CRediT authorship contribution statement

**Jiahuan Luo:** Methodology, Writing – original draft. **Jing Wang:** Conceptualization, Writing – review & editing, Validation. **Yao Guo:** Theoretical calculation and discussion. **Jiawei Zhu:** Software. **Huihui Jin:** Software. **Zhiwei Zhang:** Software. **Daojun Zhang:** XPS test and analysis. **Yongsheng Niu:** Software. **Shaogang Hou:** Software. **Jimin Du:** XPS test and analysis. **Daping He:** Visualization, Investigation. **Yuli Xiong:** Visualization, Investigation. **Lei Chen:** Visualization, Investigation. **Shichun Mu:** Conceptualization, Writing – review & editing, Validation. **Yunhui Huang:** Conceptualization, Writing – review & editing, Validation.

## Declaration of Competing Interest

The authors declare that they have no known competing financial interests or personal relationships that could have appeared to influence the work reported in this paper.

## Acknowledgments

This work was financed by the National Natural Science Foundation of China, China (Grant No. 21801005, 21901008, 22075223), Scientific and Technological Project of Henan Province, China (192102310232), Initiation Funds for Postdoctoral Scientific Research Projects in Henan Province, China (1901020), Hubei Natural Science Foundation, China (No. 2020CFB774), and the Foundation of 'Domestic visiting scholar program (2018-2019) for young backbone teachers from Colleges and universities in central and Western China, China'.

## Appendix A. Supporting information

Supplementary data associated with this article can be found in the online version at doi:10.1016/j.apcatb.2021.121043.

## References

[1] C. Wei, R.R. Rao, J. Peng, B. Huang, I.E.L. Stephens, M. Risch, J.Z. Xu, Y. Shao-Horn, Recommended practices and benchmark activity for hydrogen and oxygen electrocatalysis in water splitting and fuel cells, Adv. Mater. 31 (2019), 1806296.
[2] Staffell, I.D. Scamman, A. Velazquez Abad, P. Balcombe, P.E. Dodds, P. Ekins, N. Shah, K.R. Ward, The role of hydrogen and fuel cells in the global energy system, Energy Environ. Sci. 12 (2019) 463–491.
[3] L. Kong, M. Zhong, W. Shuang, Y. Xu, X.-H. Bu, Atomic site electrocatalysts for water splitting, oxygen reduction and selective oxidation, Chem. Soc. Rev. 49 (2020) 2215–2264.
[4] D. Zhao, Z. Zhuang, X. Cao, C. Zhang, Q. Peng, C. Chen, Y. Li, Recent advances in electrocatalytic hydrogen evolution using nanoparticles, Chem. Soc. Rev. 120 (2020) 851–918.
[5] J. Zhu, L. Hu, P. Zhao, L.Y.S. Lee, K.-Y. Wong, Recent advances in electrocatalytic hydrogen evolution using nanoparticles, Chem. Rev. 120 (2020) 851–918.
[6] J.A. Turner, Sustainable hydrogen production, Science 305 (2004) 972–974.
[7] R. Subbaraman, D. Tripkovic, K.-C. Chang, D. Strmcnik, A.P. Paulikas, P. Hirunsit, M. Chan, J. Greeley, V. Stamenkovic, N.M. Markovic, Trends in activity for the water electrolyser reactions on 3d M (Ni, Co, Fe, Mn) hydr(oxy)oxide catalysts, Nat. Mater. 11 (2012) 550–557.
[8] D. Strmcnik, M. Uchimura, C. Wang, R. Subbaraman, N. Danilovic, D. van der Vliet, A.P. Paulikas, V.R. Stamenkovic, N.M. Markovic, Improving the hydrogen

oxidation reaction rate by promotion of hydroxyl adsorption, Nat. Chem. 5 (2013) 300–306.
[9] S. Sultan, J.N. Tiwari, A.N. Singh, S. Zhumagali, M. Ha, C.W. Myung, P. Thangavel, K.S. Kim, Single atoms and clusters based nanomaterials for hydrogen evolution, oxygen evolution reactions, and full water splitting, Adv. Energy Mater. 9 (2019), 1900624.
[10] L. Liang, H. Jin, H. Zhou, B. Liu, C. Hu, D. Chen, Z. Wang, Z. Hu, Y. Zhao, H.-W. Li, D. He, S. Mu, Cobalt single atom site isolated Pt nanoparticles for efficient ORR and HER in acid media, Nano Energy 88 (2021), 106221.
[11] X. Mu, J. Gu, F. Feng, Z. Xiao, C. Chen, S. Liu, S. Mu, RuRh bimetallene nanoring as high-efficiency pH-universal catalyst for hydrogen evolution reaction, Adv. Sci. 8 (2021), 2002341.
[12] S. Yuan, Z. Pu, H. Zhou, J. Yu, I.S. Amiinu, J. Zhu, Q. Liang, J. Yang, D. He, Z. Hu, G. Van Tendeloo, S. Mu, A universal synthesis strategy for single atom dispersed cobalt/metal clusters heterostructure boosting hydrogen evolution catalysis at all pH values, Nano Energy 59 (2019) 472–480.
[13] J. Wang, L. Han, B. Huang, Q. Shao, H.L. Xin, X. Huang, Amorphization activated ruthenium-tellurium nanorods for efficient water splitting, Nat. Commun. 10 (2019) 5692.
[14] K. Eiler, S. Suriñach, J. Sort, E. Pellicer, Mesoporous Ni-rich Ni-Pt thin films: Electrodeposition, characterization and performance toward hydrogen evolution reaction in acidic media, Appl. Catal. B-Environ. 265 (2020), 118597.
[15] P.P. Li, R.B. Zhao, H.Y. Chen, H.B. Wang, P.P. Wei, H. Huang, Q. Liu, T.S. Li, X. F. Shi, Y.Y. Zhang, Liu, L.M.X.P. Sun, Recent advances in the development of water oxidation electrocatalysts at mild pH, Small 15 (2019), 180503.
[16] Q. Liang, H. Jin, Z. Wang, Y. Xiong, S. Yuan, X. Zeng, D. He, S. Mu, Metal-organic frameworks derived reverse-encapsulation Co-NC@$Mo_2C$ complex for efficient overall water splitting, Nano Energy 57 (2019) 746–752.
[17] P. Wei, X. Li, Z. He, Z. Li, X. Zhang, X. Sun, Q. Li, H. Yang, J. Han, Y. Huang, Electron density modulation of MoP by rare earth metal as highly efficient electrocatalysts for pH-universal hydrogen evolution reaction, Appl. Catal. B-Environ. 299 (2021), 120657.
[18] J. Duan, S. Chen, C.A. Ortíz-Ledón, M. Jaroniec, S.-Z. Qiao, Phosphorus vacancies that boost electrocatalytic hydrogen evolution by two orders of magnitude, Angew. Chem. Int. Ed. 59 (2020) 8181–8186.
[19] Z. Kou, W. Zang, Y. Ma, Z. Pan, S. Mu, X. Gao, B. Tang, M. Xiong, X. Zhao, A. K. Cheetham, L. Zheng, J. Wang, Cage-confinement pyrolysis route to size-controlled molybdenum-based oxygen electrode catalysts: from isolated atoms to clusters and nanoparticles, Nano Energy 67 (2020), 104288.
[20] H.Y. Kim, J.M. Kim, Y. Ha, J. Woo, A. Byun, T.J. Shin, K.H. Park, H.Y. Jeong, H. Kim, J.Y. Kim, S.H. Joo, Activity origin and multifunctionality of Pt-based intermetallic nanostructures for efficient electrocatalysis, ACS Catal. 9 (2019) 11242–11254.
[21] Z. Li, W. Niu, Z. Yang, A. Kara, Q. Wang, M. Wang, M. Gu, Z. Feng, Y. Du, Y. Yang, Simultaneous interfacial chemistry and inner Helmholtz plane regulation for superior alkaline hydrogen evolution, Energy Environ. Sci. 13 (2020) 3007–3013.
[22] K. Lu, Y. Liu, F. Lin, I.A. Cordova, S. Gao, B. Li, B. Peng, J. Kaelin, D. Coliz, C. Wang, Y. Shao, Y. Cheng, $Li_x$NiO/Ni heterostructure with strong basic lattice oxygen enables electrocatalytic hydrogen evolution with Pt-like activity, J. Am. Chem. Soc. 142 (2020) 12613–12619.
[23] J. Mahmood, F. Li, S.M. Jung, M.S. Okyay, I. Ahmad, S.J. Kim, Park, N.H.Y. Jeong, J.B. Baek, An efficient and pH-universal ruthenium-based catalyst for the hydrogen evolution reaction, Nat. Nanotechnol. 12 (2017) 441–446.
[24] Z. Pu, I.S. Amiinu, Z. Kou, W. Li, S. Mu, $RuP_2$-based catalysts with platinum-like activity and higher durability for the hydrogen evolution reaction at all pH-values, Angew. Chem. Int. Ed. 56 (2017) 11559–11564.
[25] T. Bian, B. Xiao, B. Sun, L. Huang, S. Su, Y. Jiang, J. Xiao, A. Yuan, H. Zhang, D. Yang, Local epitaxial growth of Au-Rh core-shell star-shaped decahedra: a case for studying electronic and ensemble effects in hydrogen evolution reaction, Appl. Catal. B-Environ. 265 (2020), 118255.
[26] J. Chen, M. Qin, S. Ma, R. Fan, X. Zheng, S. Mao, C. Chen, Y. Wang, Rational construction of Pt/PtTex interface with optimal intermediate adsorption energy for efficient hydrogen evolution reaction, Appl. Catal. B-Environ. 299 (2021), 120640.
[27] W. Li, Y. Liu, M. Wu, X. Feng, S.A.T. Redfern, Y. Shang, X. Yong, T. Feng, K. Wu, Z. Liu, B. Li, Z. Chen, J.S. Tse, S. Lu, B. Yang, Carbon-quantum-dots-loaded ruthenium nanoparticles as an efficient electrocatalyst for hydrogen production in alkaline media, Adv. Mater. 30 (2018), 1800676.
[28] D. Chen, T. Liu, P. Wang, J. Zhao, C. Zhang, R. Cheng, W. Li, P. Ji, Z. Pu, S. Mu, Ionothermal route to phase-pure $RuB_2$ catalysts for efficient oxygen evolution and water splitting in acidic media, ACS Energy Lett. 5 (2020) 2909–2915.
[29] Y. Qiao, P. Yuan, C.-W. Pao, Y. Cheng, Z. Pu, Q. Xu, S. Mu, J. Zhang, Boron-rich environment boosting ruthenium boride on B, N doped carbon outperforms platinum for hydrogen evolution reaction in a universal pH range, Nano Energy 75 (2020), 104881.
[30] L. Wang, Q. Zhou, Z. Pu, Q. Zhang, X. Mu, H. Jing, S. Liu, C. Chen, S. Mu, Surface reconstruction engineering of cobalt phosphides by Ru inducement to form hollow Ru-$RuP_x$-$Co_xP$ pre-electrocatalysts with accelerated oxygen evolution reaction, Nano Energy 53 (2018) 270–276.
[31] S. Jeong, H.D. Mai, T.K. Nguyen, J.-S. Youn, K.-H. Nam, C.-M. Park, K.-J. Jeon, Atomic interactions of two-dimensional $PtS_2$ quantum dots/TiC heterostructures for hydrogen evolution reaction, Appl. Catal. B-Environ. 293 (2021), 120227.
[32] T. Qiu, Z. Liang, W. Guo, S. Gao, C. Qu, H. Tabassum, H. Zhang, B. Zhu, R. Zou, Y. Shao-Horn, Highly exposed ruthenium-based electrocatalysts from bimetallic metal-organic frameworks for overall water splitting, Nano Energy 58 (2019) 1–10.
[33] F. Zhou, R. Sa, X. Zhang, S. Zhang, Z. Wen, R. Wang, Robust ruthenium diphosphide nanoparticles for pH-universal hydrogen evolution reaction with platinum-like activity, Appl. Catal. B-Environ. 274 (2020), 119092.
[34] J. Wang, W. Fang, Y. Hu, Y. Zhang, J. Dang, Y. Wu, B. Chen, H. Zhao, Z. Li, Single atom Ru doping 2H-$MoS_2$ as highly efficient hydrogen evolution reaction electrocatalyst in a wide pH range, Appl. Catal. B-Environ. 298 (2021), 120490.
[35] S. Cherevko, S. Geiger, O. Kasian, N. Kulyk, J.-P. Grote, A. Savan, B.R. Shrestha, S. Merzlikin, B. Breitbach, A. Ludwig, K.J.J. Mayrhofer, Oxygen and hydrogen evolution reactions on Ru, $RuO_2$, Ir, and $IrO_2$ thin film electrodes in acidic and alkaline electrolytes: a comparative study on activity and stability, Catal. Today 262 (2016) 170–180.
[36] W. Li, Y. Xiong, Z. Wang, M. Bao, J. Liu, D. He, S. Mu, Seed-mediated synthesis of large-diameter ternary TePtCo nanotubes for enhanced oxygen reduction reaction, Appl. Catal. B-Environ. 231 (2018) 277–282.
[37] Y. Zheng, Y. Jiao, Zhu, Y.H. Li, L.Y. Han, Y. Chen, M. Jaroniec, S.Z. Qiao, High electrocatalytic hydrogen evolution activity of an anomalous ruthenium catalyst, J. Am. Chem. Soc. 138 (2016) 16174–16181.
[38] J. Su, Y. Yang, G. Xia, J. Chen, P. Jiang, Q. Chen, Ruthenium-cobalt nanoalloys encapsulated in nitrogen-doped graphene as active electrocatalysts for producing hydrogen in alkaline media, Nat. Commun. 8 (2017) 14969.
[39] Z. Liu, Z. Li, J. Li, J. Xiong, S. Zhou, J. Liang, W. Cai, C. Wang, Z. Yang, H. Cheng, Engineering of Ru/$Ru_2P$ interfaces superior to Pt active sites for catalysis of the alkaline hydrogen evolution reaction, J. Mater. Chem. A 7 (2019) 5621–5625.
[40] T. Liu, S. Wang, Q. Zhang, L. Chen, W. Hu, C.M. Li, Ultra-small $Ru_2P$ nanoparticles on graphene: a highly efficient hydrogen evolution reaction electrocatalyst in both acidic and alkaline media, Chem. Comm. 54 (2018) 3343–3346.
[41] J.-S. Li, M.-J. Huang, Y.-W. Zhou, X.-N. Chen, S. Yang, J.-Y. Zhu, G.-D. Liu, L.-J. Ma, S.-H. Cai, J.-Y. Han, $RuP_2$-based hybrids derived from MOFs: highly efficient pH-universal electrocatalysts for the hydrogen evolution reaction, J. Mater. Chem. A 9 (2021) 12276–12282.
[42] N. Hanikel, X. Pei, S. Chheda, H. Lyu, W. Jeong, J. Sauer, L. Gagliardi, O.M. Yaghi, Evolution of water structures in metal-organic frameworks for improved atmospheric water harvesting, Science 374 (2021) 454–459.
[43] L. Hu, R. Xiao, X. Wang, X. Wang, C. Wang, J. Wen, W. Gu, C. Zhu, MXene-induced electronic optimization of metal-organic framework-derived CoFe LDH nanosheet arrays for efficient oxygen evolution, Appl. Catal. B-Environ. 298 (2021), 120599.
[44] Y.-N. Gong, J.-H. Mei, J.-W. Liu, H.-H. Huang, J.-H. Zhang, X. Li, D.-C. Zhong, T.-B. Lu, Manipulating metal oxidation state over ultrastable metal-organic frameworks for boosting photocatalysis, Appl. Catal. B-Environ. 292 (2021), 120156.
[45] S. Karamzadeh, E. Sanchooli, A.R. Oveisi, S. Daliran, R. Luque, Visible-LED-light-driven photocatalytic synthesis of N-heterocycles mediated by A polyoxometalate-containing mesoporous zirconium metal-organic framework, Appl. Catal. B-Environ. (2021), 120815.
[46] K. An, H. Ren, D. Yang, Z. Zhao, Y. Gao, Y. Chen, J. Tan, W. Wang, Z. Jiang, Nitrogenase-inspired bimetallic metal organic frameworks for visible-light-driven nitrogen fixation, Appl. Catal. B-Environ. 292 (2021), 120167.
[47] Y. Xu, M. Liu, M. Wang, T. Ren, K. Ren, Z. Wang, X. Li, L. Wang, H. Wang, Methanol electroreforming coupled to green hydrogen production over bifunctional NiIr-based metal-organic framework nanosheet arrays, Appl. Catal. B-Environ. 300 (2022), 120753.
[48] O. Kozachuk, K. Yusenko, H. Noei, Y. Wang, S. Walleck, T. Glaser, R.A. Fischer, Solvothermal growth of a ruthenium metal-organic framework featuring HKUST-1 structure type as thin films on oxide surfaces, Chem. Commun. 47 (2011) 8509–8511.
[49] Z. Pu, J. Zhao, I.S. Amiinu, W. Li, M. Wang, D. He, S. Mu, A universal synthesis strategy for P-rich noble metal diphosphide-based electrocatalysts for the hydrogen evolution reaction, Energy Environ. Sci. 12 (2019) 952–957.